nature communications

Article

https://doi.org/10.1038/s41467-025-57446-w

Monitoring mRNA vaccine antigen expression in vivo using PET/CT

Received: 11 June 2024

Accepted: 20 February 2025

Published online: 06 March 2025

Check for updates

Gabrielle S. Blizard[1,2], Garima Dwivedi[3,4], Yi-Gen Pan[3], Catherine Hou[1], Jean M. Etersque[1,2], Hooda Said[5], Anik Chevrier[6], Marc Lavertu[6], Houping Ni[3,4], Benjamin Davis[3,4], Ying Tam[7], Quy Cao[8], Robert H. Mach[1], Drew Weissman[3,4], Mohamad-Gabriel Alameh[3,4,5,9] ✉ & Mark A. Sellmyer[1,2] ✉

Noninvasive visualization of the distribution and persistence of mRNA vaccine antigen expression in mammalian systems has implications for the development and evaluation of future mRNA vaccines. Here, we genetically fuse *E. coli* dihydrofolate reductase (eDHFR) to the delta furin diproline modified SARS-CoV-2 spike glycoprotein ($S2P^{\Delta f}$) mRNA vaccine and image its expression in female mice and male non-human primates using [^{18}F]fluoropropyl-trimethoprim ([^{18}F]FP-TMP). Whole body positron emission tomography (PET) imaging revealed transient expression of the vaccine antigen in the injection site and draining lymph nodes (dLNs). Fusion of eDHFR did not impact S2P immunogenicity and no humoral or cellular immune response was detected against eDHFR in either species. In this work, we show that eDHFR can be used as an mRNA-encoded PET reporter gene to monitor the spatiotemporal dynamics of mRNA vaccine antigen expression in vivo. This technique could be applied in clinical translation of future mRNA vaccines or therapeutics.

The rapid production of mRNA vaccines allows for flexibility in testing multiple candidate antigens during the development process[1]. As the minimal genetic vector, in vitro transcribed mRNA is transiently translated into functional protein products upon release in the cytoplasm and degraded by normal cellular processes[2]. Given the broad scope of diseases with potential to be treated by mRNA vaccines, efficient in vivo delivery and cellular expression in target tissues is crucial and achieved through formulation of mRNA into carrier molecules such as lipid nanoparticles (LNPs)[3]. Optimization of the mRNA transcript as well as altering the tissue tropism of LNPs through lipid composition or addition of a targeting moiety has been used to boost translation and target specific cells[4–6]. Additionally, vaccines are typically evaluated via several delivery routes which can further influence expression kinetics and tissue tropism[7]. Noninvasive approaches to measure the biodistribution of mRNA expression longitudinally after in vivo delivery would be particularly powerful to evaluate future mRNA vaccine formulations and to optimize dosing in Phase I/II clinical trials.

Most methods to assess protein expression in a living subject require fixed tissues obtained invasively through biopsy or terminal endpoints, precluding longitudinal evaluation[8]. Conversely, reporter genes are especially useful tools for noninvasive monitoring of molecular events such as transcription and translation within living organisms. A reporter gene encodes a protein product which produces an observable output upon excitation or interaction with its substrate pair[9]. Delivery of optical reporters such as luciferase has been used to

[1]Department of Radiology, Perelman School of Medicine, University of Pennsylvania, Philadelphia, PA, USA. [2]Department of Biochemistry and Biophysics, Perelman School of Medicine, University of Pennsylvania, Philadelphia, PA, USA. [3]Division of Infectious Diseases, Perelman School of Medicine, University of Pennsylvania, Philadelphia, PA, USA. [4]Penn Institute for RNA Innovation, Perelman School of Medicine, University of Pennsylvania, Philadelphia, PA, USA. [5]Department of Pathology, Children's Hospital of Philadelphia, Philadelphia, PA, USA. [6]Chemical Engineering Department, Polytechnique Montreal, Montreal, QC, Canada. [7]Acuitas Therapeutics, Vancouver, BC, Canada. [8]Department of Biostatistics, Epidemiology, and Informatics, Perelman School of Medicine, University of Pennsylvania, Philadelphia, PA, USA. [9]Department of Pathology and Laboratory Medicine, Perelman School of Medicine, University of Pennsylvania, Philadelphia, PA, USA. ✉e-mail: mg.alameh@pennmedicine.upenn.edu; mark.sellmyer@pennmedicine.upenn.edu

assess live animal biodistribution of mRNA-LNPs following administration in mice via different routes[10]. Attempts to assess transfection on a cellular level have delivered mRNA expressing Cre recombinase in transgenic mouse lines to activate genetic reporters such as tdTomato[11]. While these are potent tools in cell-based or small animal models, they are not useful in deep tissues, large animal models, or in human participants[12].

Positron emission tomography (PET) is a clinically established imaging modality used for quantitative measures of radiotracer accumulation in tissues[13]. In tandem with computed tomography (CT), PET/CT is a powerful technique with high spatial resolution, combining 3D anatomical data with precise radiotracer localization and occupancy. Existing PET reporter systems, such as the sodium iodide symporter (NIS), have been engineered to report on the presence of RNA molecules using a repressor-based strategy[14]. Other groups have used radiolabeled metabolite analogs to monitor response to therapeutic mRNAs[15]. In the context of mRNA-LNPs, direct radiolabeling of LNPs has been employed to monitor their biodistribution following systemic administration[16]. An alternative is to radiolabel the nucleic acid directly. For example, an mRNA vaccine encoding the yellow fever *prME* proteins was directly labeled with ^{64}Cu and complexed with lipid derivatives for intramuscular administration in non-human primates (NHPs)[17]. Using PET/CT, the mRNA transcript was visualized trafficking from the site of injection to the dLNs over a 28 h time course. However, none of these approaches enable in vivo observation of the downstream mRNA translation and corresponding protein expression, which produces the key bioactive species.

Here, we present an mRNA-encoded PET reporter gene for longitudinal monitoring of protein expression in vivo for vaccine research and development. We chose the highly specific enzyme-inhibitor pair comprised of *Escherichia coli* dihydrofolate reductase (eDHFR) and small molecule antibiotic trimethoprim (TMP) as our PET reporter system. Our choice for this PET reporter system was informed by our previous work in which we developed TMP-based radiotracers, ([^{18}F]FP-TMP and [^{11}C]-TMP) and imaged eDHFR-expressing chimeric antigen receptor (CAR) T cells in mice and bacterial infections in humans, respectively[18,19]. eDHFR is an ideal protein tag as it is small (18 kDa) and monomeric[20]. Additionally, [^{18}F]FP-TMP binds tightly with eDHFR (K_d = 0.465 nM) and functions orthogonally in mammalian systems as TMP is over 10,000-fold more selective for eDHFR than the mammalian protein homolog[21,22]. Using the delta furin diproline modified (prefusion-stabilized) SARS-CoV-2 spike glycoprotein (S2P$^{\Delta f}$) as our vaccine prototype, eDHFR was genetically fused at the C-terminal end and imaged using [^{18}F]FP-TMP to assess biodistribution and translation persistence of the antigen in whole body systems. This PET imaging approach has potential for rapid screening of future mRNA vaccines and therapeutics in both small and large animal models and could be applied in investigational clinical trials to guide our understanding of mRNA-LNP pharmacokinetics (PK) and pharmacodynamics (PD).

Results

S2P$^{\Delta f}$-eDHFR maintains membrane localization and specific [^{18}F]FP-TMP binding in cells

To prevent cleavage and the uncoupling of the reporter protein (eDHFR) from the immunogenic species (S2P), the furin cleavage site was deleted from S2P and eDHFR was genetically fused to the C-terminus (S2P$^{\Delta f}$-eDHFR) for PET imaging (Fig. 1a, b). To validate genetic fusion and confirm deletion of the cleavage site, we transfected S2P and S2P$^{\Delta f}$-eDHFR mRNA into HEK293T cells. At 24 h, cells were lysed and blotted for S2P using a mouse monoclonal antibody against the S2 domain of the SARS-CoV-2 spike glycoprotein. S2P$^{\Delta f}$-eDHFR protein showed an approximate +18 kDa shift relative to S2P suggesting successful genetic fusion of our PET reporter (Fig. 1c). A second band was detected in the S2P lysate corresponding to a glycosylated S2 cleavage product while no cleavage product was observed in the S2P$^{\Delta f}$-eDHFR lysate. Next, to assess proper cellular membrane localization of S2P$^{\Delta f}$-eDHFR in mammalian cells, we transfected HEK293T and DC2.4 cells, an immortalized mouse dendritic cell line, then stained with a fluorescent S2 antibody and analyzed by flow cytometry. Cells transfected with S2P and S2P$^{\Delta f}$-eDHFR demonstrated an increase in fluorescence compared with non-transfected cells suggesting surface expression of the S2P$^{\Delta f}$-eDHFR fusion protein (Fig. 1d, Supplementary Fig. 1). Greater fluorescence was observed in cells expressing S2P compared with S2P$^{\Delta f}$-eDHFR, likely resulting from improved surface trafficking of the canonical sequence. Finally, as proof-of-concept, we incubated [^{18}F]FP-TMP with HEK293T cells expressing S2P or S2P$^{\Delta f}$-eDHFR. Cells expressing S2P$^{\Delta f}$-eDHFR demonstrated a 20-fold increase in radiotracer uptake compared to cells expressing S2P alone. Co-incubation with a molar excess of unlabeled TMP abrogated uptake of [^{18}F]FP-TMP, confirming specificity of our radiotracer for eDHFR (Fig. 1e).

PET/CT detection of S2P$^{\Delta f}$-eDHFR expression in the dLNs and injected muscle of mice

S2P$^{\Delta f}$-eDHFR expression was monitored in mice using PET/CT. Mice were intramuscularly (IM) administered either empty LNPs (eLNPs) or S2P$^{\Delta f}$-eDHFR mRNA-LNPs in the right hindlimb on day 0 and imaged with [^{18}F]FP-TMP on day 1 and 3 (Fig. 2a). To determine protein expression, a 3D region of interest (ROI) was drawn over the injected muscle and ipsilateral popliteal LN and the maximum standard uptake value (SUV_{max}) of [^{18}F]FP-TMP was quantified (Supplementary Fig. 2). There was significant uptake of [^{18}F]FP-TMP in the muscle ($p = 0.0002$) and ipsilateral popliteal LN ($p < 0.0001$) of mice vaccinated with S2P$^{\Delta f}$-eDHFR on day 1 which decreased to background by day 3, indicative of the transient nature of mRNA-mediated protein expression and the protein recycling half-life (Fig. 2b, c). No uptake was observed in the mice injected with eLNP at either timepoint. To confirm that [^{18}F]FP-TMP uptake was specific for eDHFR and not an artifact of vaccine-mediated inflammation, we vaccinated mice with either S2P or S2P$^{\Delta f}$-eDHFR mRNA-LNPs and performed PET/CT imaging on day 1. There was an 8-fold increase in uptake of [^{18}F]FP-TMP in the ipsilateral popliteal LN ($p < 0.0001$) and a 6-fold increase in uptake in the injected muscle ($p < 0.0001$) in mice vaccinated with S2P$^{\Delta f}$-eDHFR compared to mice vaccinated with S2P (Fig. 2d–f). The difference observed in injected muscle uptake between imaging studies suggests variability in the timing and way muscle cells are transfected following mRNA-LNP vaccination, while the dLNs remain a reliable tissue compartment for vaccine antigen expression. These results are consistent with an ex vivo biodistribution experiment in which [^{18}F]FP-TMP uptake was detected specifically in the ipsilateral dLNs and muscle of S2P$^{\Delta f}$-eDHFR vaccinated mice. The eDHFR control did not appear to express well as no statistical increase in [^{18}F]FP-TMP uptake was present (Supplementary Fig. 3). S2P and eDHFR expression in the ipsilateral dLNs was confirmed by flow cytometry using a fluorescent S2 antibody and a fluorescent TMP derivative (TMP-JF646), respectively (Supplementary Figs. 4–5).

S2P retains immunogenicity while eDHFR elicits no humoral or cellular response in mice

We next investigated the ability of S2P$^{\Delta f}$-eDHFR to elicit an immune response to ensure that eDHFR had no detrimental impact on S2P immunogenicity and to test whether eDHFR, expressed as a cytosolic fusion protein to S2P, had any immunogenicity itself. Mice were vaccinated with eDHFR, S2P$^{\Delta f}$-eDHFR, or S2P mRNA-LNPs on day 0 and boosted on day 21. On day 21 and 35, whole blood was collected from mice and serum separated for analysis via endpoint ELISA (Fig. 3a). At all timepoints, high levels of total IgG antibodies against SARS-CoV-2 spike glycoprotein were detected in mice that received S2P$^{\Delta f}$-eDHFR or S2P vaccination but not in mice that received an eDHFR vaccination (Fig. 3b). As expected, we observed an increase in immune response

https://doi.org/10.1038/s41467-025-57446-w

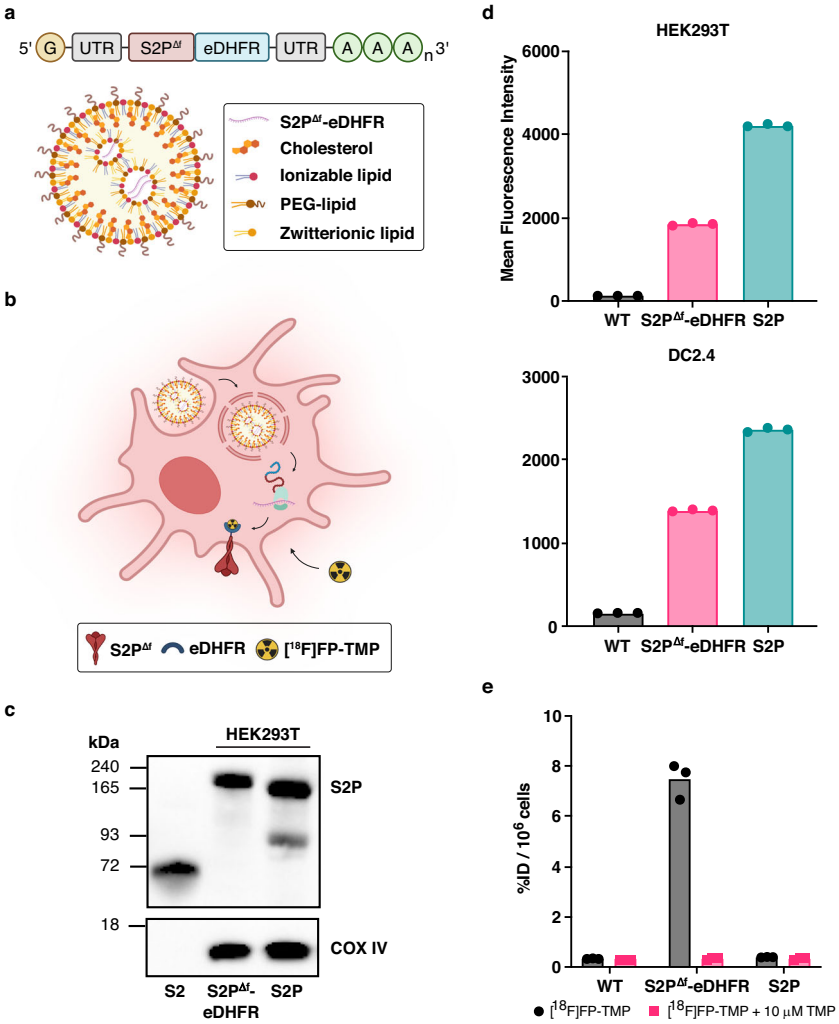

Fig. 1 | Expression of S2P$^{\Delta f}$-eDHFR and specific uptake of [^{18}F]FP-TMP in mammalian cells. a N1Ψ-modified mRNA encoding the delta furin diproline modified SARS-CoV-2 spike glycoprotein (S2P$^{\Delta f}$) was genetically fused to eDHFR and formulated in LNPs containing cholesterol, an ionizable lipid, a PEG-lipid, and DSPC as a zwitterionic lipid (not to scale). **b** LNPs transfect antigen-presenting cells (APCs) and mRNA is released and translated into S2P$^{\Delta f}$-eDHFR. Cells expressing the fusion antigen can be imaged using [^{18}F]FP-TMP. **c** Confirmation of S2P$^{\Delta f}$-eDHFR fusion by Western blot with an anti-spike antibody. eDHFR adds an 18 kDa shift to the molecular weight. Recombinant spike S2 protein produced in insect cells was used as a positive control, 59 kDa. COX IV was used as a loading control, 18 kDa. Representative data from $n = 3$ independent experiments. **d** Mean fluorescence intensity of HEK293T and DC2.4 cells expressing S2P$^{\Delta f}$-eDHFR or S2P and labeled with an anti-spike AF647 conjugated antibody. Data shown is $n = 3$ technical replicates representative of three independent experiments. **e** Uptake of [^{18}F]FP-TMP in HEK293T cells transfected with S2P$^{\Delta f}$-eDHFR or S2P mRNA. Cold TMP (10 μM) was used as a blocking agent. Data is shown as %ID per 1e6 cells. Data shown is $n = 3$ technical replicates representative of two independent experiments. Data presented as mean. **a**, **b** Created in BioRender. Sellmyer, M. (2025) https://BioRender.com/x00q954. Source data for panel (**c**–**e**) are provided as a Source Data file.

against spike between prime and boost which is comparable between S2P$^{\Delta f}$-eDHFR and S2P. No antibodies were detected against eDHFR in any of the groups at either timepoint. (Fig. 3c). These data are consistent with results obtained from a separate experiment conducted with alternative controls including a cohort injected with eLNP (Supplementary Fig. 6). Spleens were collected and splenocytes were isolated for further profiling of antigen-specific CD4$^+$ and CD8$^+$ T cells and their polyfunctionality by immunoflow cytometry (Supplementary Fig. 7). Single cell splenocytes from mice administered eLNP or S2P$^{\Delta f}$-eDHFR were stimulated in the presence of overlapping peptide pools covering the full length of either the spike or the eDHFR protein (Supplementary Table 1). As expected, significant levels of cytokine expressing T cells ($p < 0.0001$) were observed in S2P$^{\Delta f}$-eDHFR vaccinated mice following stimulation with pooled spike peptides but not towards any of the individual eDHFR peptides at prime or boost (Fig. 4a–c; Supplementary Fig. 8). Similarly, significant CD4$^+$ and CD8$^+$ T cell reactivity ($p = 0.0032$ to $p < 0.0001$) was detected against pooled spike peptides but not pooled eDHFR peptides in the S2P and S2P$^{\Delta f}$-eDHFR groups while no response to either antigen was detected in the eDHFR group (Fig. 4d, e, Supplementary Fig. 9).

In vivo cytotoxicity against spike but not eDHFR after vaccination in mice

To assess functionality of the antigen-specific CD4$^+$ and CD8$^+$ responses observed in the polyfunctional studies and further demonstrate that eDHFR is nonimmunogenic, we performed an in vivo cell killing assay by transferring peptide-loaded splenocytes into S2P$^{\Delta f}$-eDHFR vaccinated mice and monitoring cell killing. Vaccinated mice were injected with a 1:1 ratio of unstimulated splenocytes (CFSE^{lo}) to splenocytes loaded with either spike or eDHFR peptides (CFSE^{hi}) and cell killing was assessed after 24 h (Fig. 5a, b). No change in the ratio of CFSE^{lo} or CFSE^{hi} (spike- or eDHFR-loaded) splenocytes was observed in eLNP vaccinated mice (Fig. 5c–f; Supplementary Table 2) indicating absence of antigen-specific T cell killing. In S2P$^{\Delta f}$-eDHFR vaccinated

https://doi.org/10.1038/s41467-025-57446-w

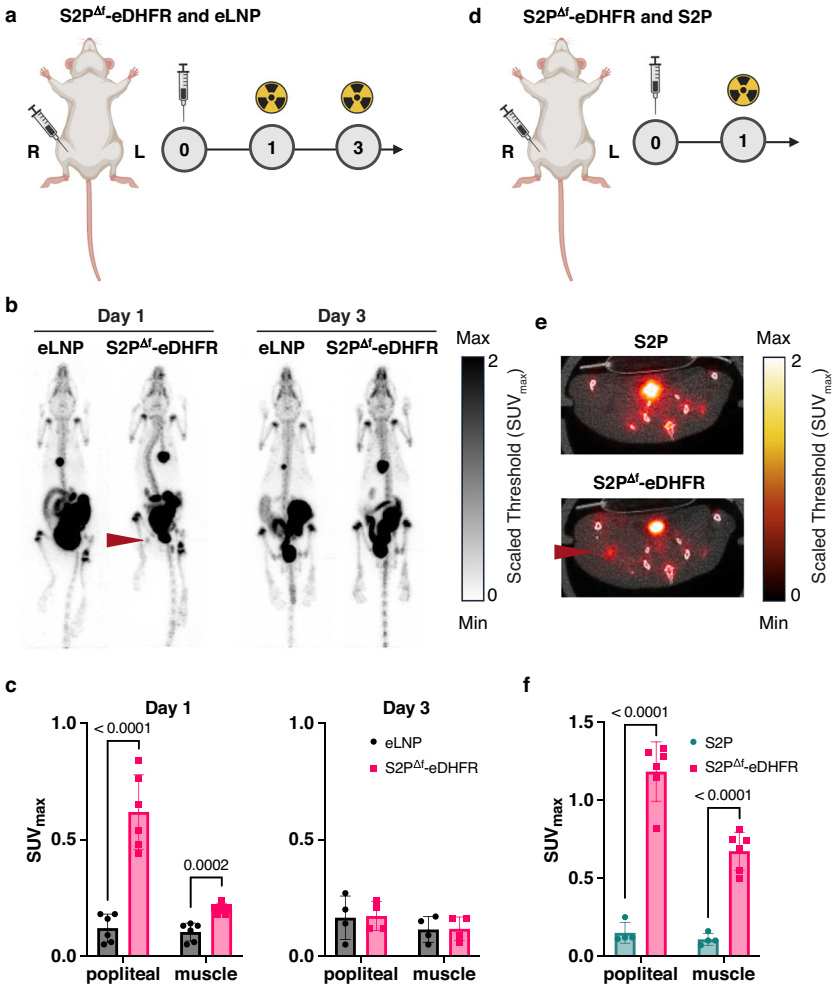

Fig. 2 | Longitudinal PET imaging in vaccinated mice. a Experimental timeline. Balb/c mice were IM injected with eLNP or S2P$^{\Delta f}$-eDHFR mRNA-LNPs in the right hindlimb on day 0. On day 1 and 3 mice were IV administered [^{18}F]FP-TMP and PET/CT images were acquired. **b** Representative PET/CT images of mice on day 1 and 3. Red arrow indicates [^{18}F]FP-TMP signal in the ipsilateral popliteal LN of the S2P$^{\Delta f}$-eDHFR vaccinated mouse on day 1. **c** [^{18}F]FP-TMP SUV$_{max}$ quantification in the ipsilateral LN and injected muscle on day 1 ($n = 6$ mice per group) and day 3 ($n = 4$ mice per group). **d** Experimental timeline of follow up experiment. Balb/c mice were vaccinated with S2P or S2P$^{\Delta f}$-eDHFR mRNA-LNPs and imaged on day 1. **e** Representative axial PET/CT slices through the popliteal LNs. Red arrow indicates [^{18}F]FP-TMP signal in the ipsilateral popliteal LN of the S2P$^{\Delta f}$-eDHFR vaccinated mouse. **f** [^{18}F]FP-TMP SUV$_{max}$ quantification in the ipsilateral LN and injected muscle on day 1 (S2P, $n = 4$; S2P$^{\Delta f}$-eDHFR, $n = 6$ mice per group). The ALC-307 lipid was used in these experiments. Groups were compared using an unpaired, two-tailed t test. Only significant pairwise comparisons are shown. Data presented as mean ± SD. (**c**, **f**) $p < 0.0001$ unless otherwise stated. day 1: muscle, $p = 0.0002$. **a**, **d** Created in BioRender. Sellmyer, M. (2025) https://BioRender.com/d90y830. Source data for panel (**c**, **f**) are provided as a Source Data file.

mice, the ratio between CFSE^{lo} and CFSE$^{hi\text{-}eDHFR}$ splenocytes was also unchanged, confirming the absence of T-cell mediated immune response against eDHFR (Fig. 5e, f; Supplementary Table 2). In contrast, nearly 80% of CFSE$^{hi\text{-}spike}$ splenocytes were killed indicating a strong and specific T cell-mediated immune response against spike (Fig. 5c-d; Supplementary Table 2).

S2P$^{\Delta f}$-eDHFR expression is detected by PET/CT imaging in NHPs

Because eDHFR was not immunogenic in mice and to demonstrate potential clinical applications, we performed longitudinal imaging of S2P$^{\Delta f}$-eDHFR in non-human primates (NHP). Two NHPs were vaccinated IM in the right deltoid and dynamic PET/CT images were acquired over a 120 min period (Fig. 6a, Supplementary Fig. 10). There was rapid accumulation of [^{18}F]FP-TMP in the ipsilateral axillary LN which increased over the 120 min time course in both NHPs on day 1 (Fig. 6b, Supplementary Fig. 10, Supplementary Movie 1). S2P$^{\Delta f}$-eDHFR expression decreased from day 1 but was still detected by PET on day 7 (Supplementary Movie 2) and 8 and was no longer detected by day 35 (Supplementary Movie 3) and 99 in NHP 1 and 2, respectively (Fig. 6b–d, Supplementary Fig. 10). There was variability in uptake of [^{18}F]FP-TMP in the injected muscle in which high muscle signal was observed in NHP 1 on day 1 but not in NHP 2 (Fig. 6b, d, Supplementary Fig. 10). Importantly, no signal was detected in the LN or the injected muscle of the *C. diff* vaccinated NHP (Fig. 6e–h). Background uptake of [^{18}F]FP-TMP in the liver, spleen, and spine was similar in all NHPs (Supplementary Figs. 11-13). Accumulation of [^{18}F]FP-TMP in the spine of NHPs has been previously reported as likely attributable to some degree of specific radiotracer accumulation in areas of hematopoietic bone marrrow[22]. No uptake was detected in the brain or gonads (Supplementary Fig. 14).

No immune response is detected against eDHFR in NHPs

The total IgG antibodies in NHP serum against spike and eDHFR were quantified post-prime and post-boost. While an increase in total IgG antibodies against spike was observed between timepoints, no antibodies were detected against eDHFR at either timepoint consistent with our previous data in mice (Fig. 7a). An ELISPOT was performed to evaluate cellular immune responses against spike and eDHFR post-

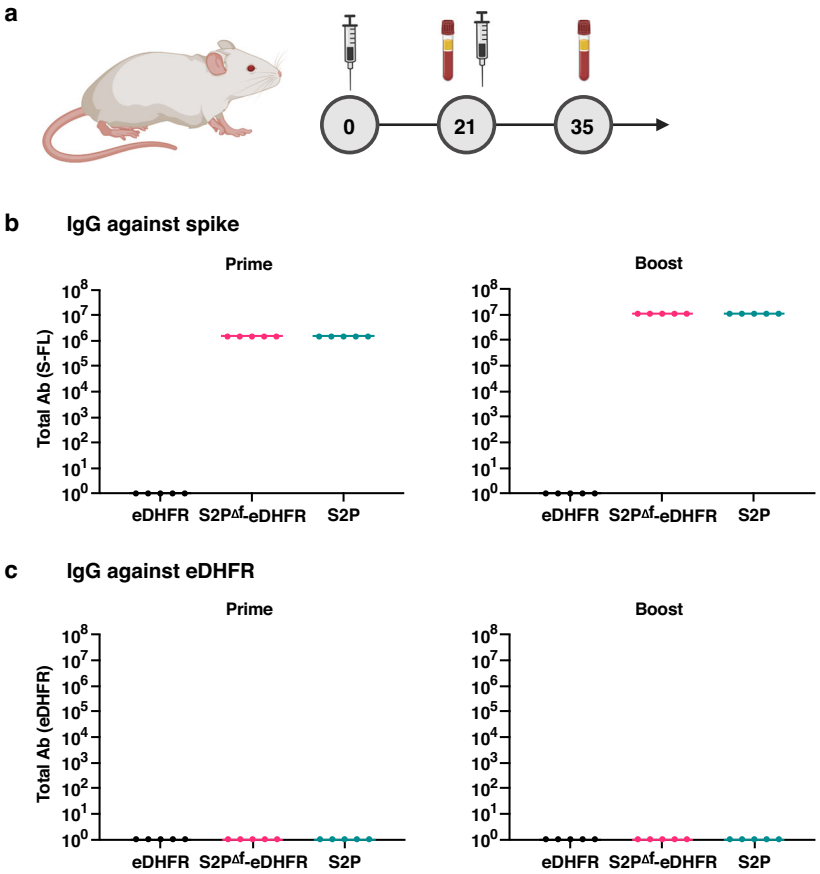

Fig. 3 | Quantification of antibodies against spike and eDHFR in mouse serum at prime and boost. a Experimental timeline. Balb/c mice were vaccinated with eDHFR, S2P$^{\Delta f}$-eDHFR, or S2P mRNA-LNPs on day 0 and 21 ($n = 5$ mice per group). On day 21 and 35 serum was collected for analysis. The ALC-0315 lipid was used in this experiment. **b** Total IgG antibodies against full length spike and **c** eDHFR protein in serum of vaccinated mice at day 21 (prime) and 35 (boost). Data presented as mean. **a** Created in BioRender. Sellmyer, M. (2025) https://BioRender.com/w43k765. Source data for panel (**b**, **c**) are provided as a Source Data file.

boost. An antigen-specific response was detected against spike with increased levels of IFN-γ and IL-2 secreting cells following stimulation (Fig. 7b, c). Conversely, no response above background was detected against any of the eDHFR peptides or the combined pool (Fig. 7b, c). A lower immune response against spike was observed in NHP 1 across assays.

Discussion

Following FDA approval of mRNA-LNP vaccines during the COVID-19 pandemic there has been a substantial increase in mRNA vaccines and therapeutics advancing toward the clinic[23–26]. Development of a clinically translatable imaging technique for in vivo monitoring of mRNA-mediated protein expression is an important step in understanding their biodistribution, pharmacokinetic and pharmacodynamic (PK/PD) profiles, and persistence in whole body systems. While current reporter gene imaging techniques that have been applied to visualizing mRNA expression (bioluminescence and fluorescence) work well in small animal models, they are incompatible with larger animals or early phase human clinical protocols. In contrast to optical mRNA imaging approaches, PET/CT provides superior spatial resolution and is translatable to the clinic given the widely available nuclear medicine infrastructure. Here, we present a straightforward PET imaging strategy for longitudinal monitoring of mRNA vaccine antigen expression using eDHFR as a reporter gene.

Several PET reporter systems have been used in clinical settings[13,27]. As a clinically approved small molecule, trimethoprim (TMP) is especially attractive and we have previously demonstrated ideal absorption, distribution, metabolism, and excretion (ADME) properties of TMP-based radiotracers in mammalian systems, including humans[18,19,22,28]. The relatively short half-life of fluorine-18 (110 min) permits repeat tracer administration for longitudinal imaging studies. Furthermore, genetic fusion of eDHFR as a small tag to the antigen of interest enables a direct relationship for quantification of protein expression through non-covalent binding of [^{18}F]FP-TMP to eDHFR. Other PET reporter systems with alternate mechanisms of tracer accumulation, such as through membrane transporters or enzymatic intracellular trapping, may have other considerations (e.g. enzymatic amplification) when being used for a quantitative readout of protein expression[29].

We chose the diproline modified SARS-CoV-2 spike glycoprotein (S2P) as our vaccine model because it has been widely administered in the approved mRNA-LNP vaccines during the COVID-19 pandemic[30]. The SARS-CoV-2 spike glycoprotein is membrane bound with the S2 domain containing the transmembrane region[31]. Surface staining of mammalian cells transfected with S2P$^{\Delta f}$-eDHFR was performed using a fluorescent antibody against the S2 region. The results demonstrated proper cellular localization of the spike protein, suggesting C-terminal fusion of eDHFR had little impact on protein folding and processing. However, lower membrane expression was observed compared to S2P alone. This result was consistent in vivo in which dendritic cells from S2P$^{\Delta f}$-eDHFR vaccinated mouse LNs had less S2P positivity than S2P vaccinated mice (Supplementary Fig. 5). As previously mentioned, this may be due to improved surface trafficking afforded by the canonical furin cleavage site present in S2P.

PET imaging of S2P$^{\Delta f}$-eDHFR in mice revealed expression in the injected muscle and the ipsilateral popliteal LN on day 1 following

https://doi.org/10.1038/s41467-025-57446-w

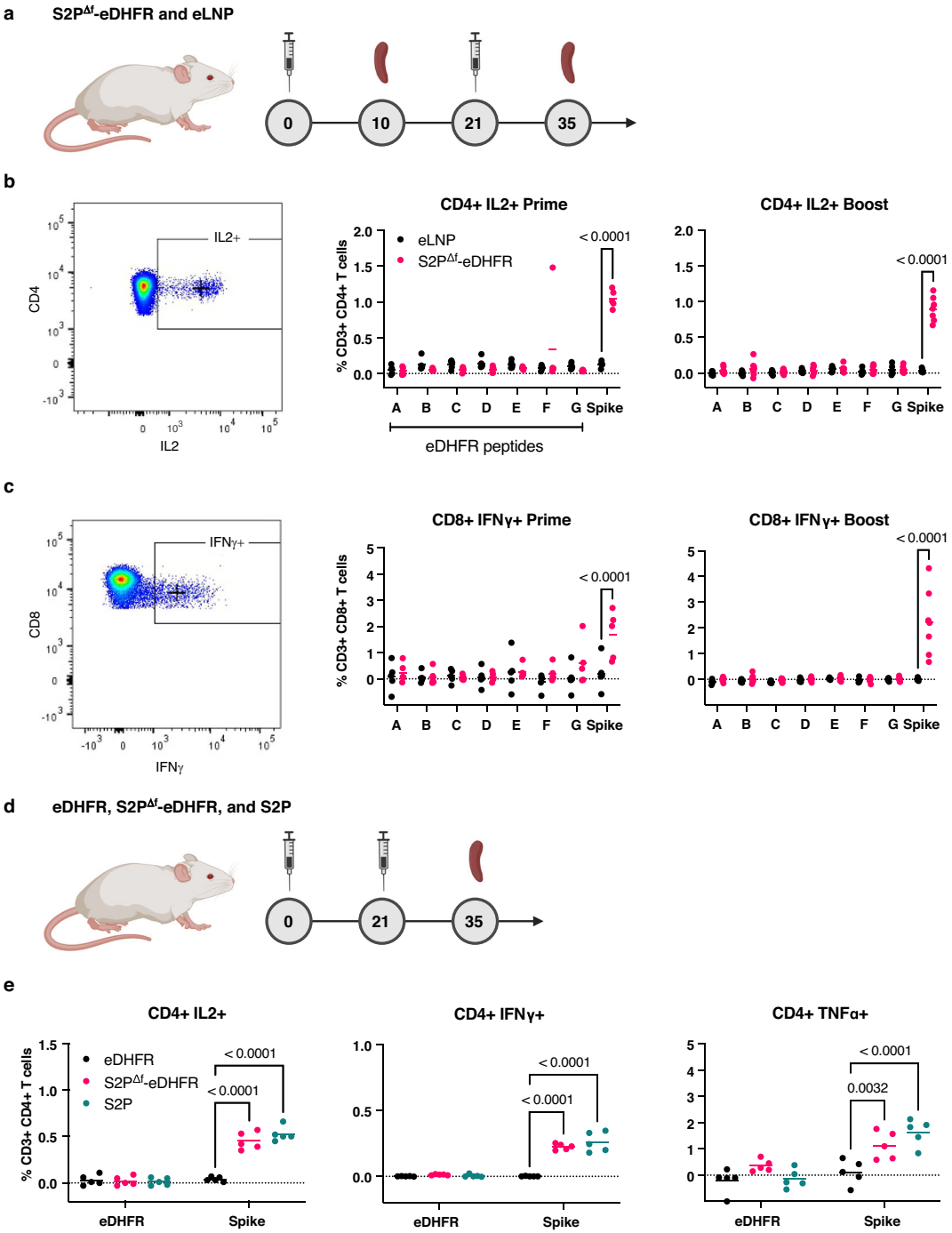

Fig. 4 | T cell polyfunctionality against spike and eDHFR. a Experimental timeline. Balb/c mice were vaccinated with eLNP or S2P$^{\Delta f}$-eDHFR mRNA-LNPs on day 0 and 21. On day 10 and 35 spleens were collected for analysis. The ALC-307 lipid was used in this experiment. **b** Representative flow plots (spike-stimulated) and quantification of CD4$^+$ IL2$^+$ and **c** CD8$^+$ IFN-γ$^+$ antigen-specific T cells after stimulation with eDHFR and spike peptides at prime (eLNP, $n = 5$; S2P$^{\Delta f}$-eDHFR, $n = 5$ mice per group) and boost (eLNP, $n = 5$; S2P$^{\Delta f}$-eDHFR, $n = 7$ mice per group). Groups were compared using a two-way ANOVA with Sidak's multiple comparisons test. **d** Experimental timeline. Balb/c mice were vaccinated with eDHFR, S2P$^{\Delta f}$-eDHFR, or S2P mRNA-LNPs on day 0 and 21 and spleens were collected on day 35 for analysis. The ALC-0315 lipid was used in this experiment. **e** Quantification of antigen-specific CD4$^+$ T cells following stimulation with eDHFR or spike. $n = 5$ mice per group. Groups were compared using a two-way ANOVA with Tukey's multiple comparisons test. Only significant pairwise comparisons are shown. Data presented as mean. (**b**, **c**, **e**) $p < 0.0001$ unless otherwise stated. Anti-spike CD4$^+$ TNF-α$^+$: eDHFR vs S2P$^{\Delta f}$-eDHFR, $p = 0.0032$. **a**, **d** Created in BioRender. Sellmyer, M. (2025) https://BioRender.com/a98s821. Source data for panel (**b**, **c**, **e**) are provided as a Source Data file.

vaccination, consistent with established mRNA-LNP dynamics in vivo[32]. Two main mechanisms have been identified by which the current mRNA-LNPs vaccines transfect the dLNs: first, they are internalized by antigen-presenting cells (APCs) at the injection site which then traffic to the dLNs; and second, the mRNA-LNPs themselves traffic to the dLNs where they are taken up by APCs directly[33]. S2P$^{\Delta f}$-eDHFR was no longer detected in any tissues by day 3, underscoring the transient nature of mRNA-mediated protein expression, especially in mice. In all mice, there was typical [^{18}F]FP-TMP background uptake in the bone and gastrointestinal tract which we have previously reported as related

https://doi.org/10.1038/s41467-025-57446-w

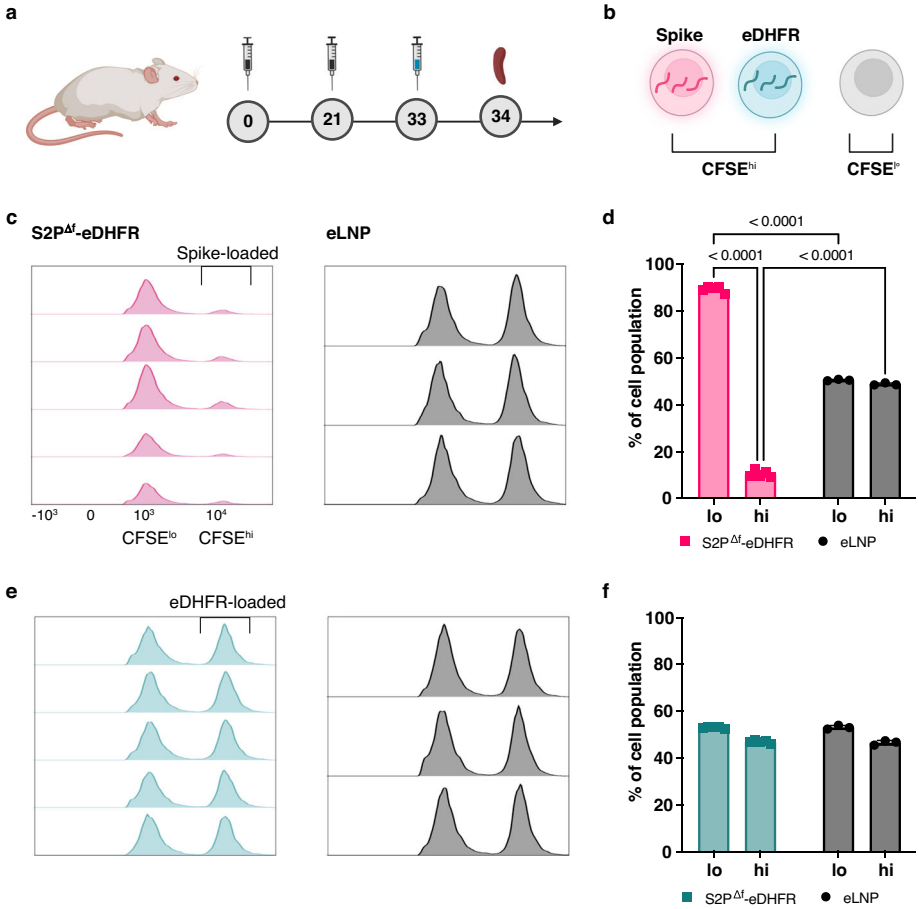

Fig. 5 | In vivo cytotoxicity against splenocytes loaded with spike or eDHFR peptides. a Experimental timeline. Balb/c mice were vaccinated with eLNP or S2P$^{\Delta f}$-eDHFR mRNA-LNPs on day 0 and boosted on day 21. On day 33 mice were IV injected with a 1:1 ratio of unstimulated and peptide-loaded syngeneic splenocytes and sacrificed on day 34 for analysis. The ALC-307 lipid was used in this experiment. **b** Schematic of peptide-loaded splenocytes. **c** Flow plot populations of unstimulated (CFSE^{lo}) and spike-loaded (CFSE^{hi}) splenocytes and **d** quantification. **e** Flow plot populations of unstimulated (CFSE^{lo}) and eDHFR-loaded (CFSE^{hi}) splenocytes and **f** quantification. Position of loaded splenocytes and CFSE^{lo} and CFSE^{hi} cell populations are indicated on the S2P$^{\Delta f}$-eDHFR vaccinated flow plots. S2P$^{\Delta f}$-eDHFR, $n = 5$; eLNP $n = 3$ mice per group. CFSE^{lo} and CFSE^{hi} groups were compared using a two-way ANOVA with Sidak's multiple comparisons test. Only significant pairwise comparisons are shown. Data presented as mean ± SD. **d** $p < 0.0001$ unless otherwise stated. **a**, **b** Created in BioRender. Sellmyer, M. (2025) https://BioRender.com/p80q175. Source data for panel (**d**, **f**) are provided as a Source Data file.

to a component of rodent-specific defluorination of the radiotracer and normal excretion processes, respectively[18,19].

Clinically it has been shown that [^{18}F]-fluorodeoxyglucose (FDG), a glucose analog taken up by metabolically active cells, accumulates in sites of inflammation including the dLNs ipsilateral to vaccination[34,35]. While [^{18}F]-FDG accumulates in hypermetabolic cells nonspecifically, [^{18}F]FP-TMP binds specifically to eDHFR. We have previously shown that [^{18}F]FP-TMP is not taken up by sterile inflammation, suggesting that the muscle and LN signal detected in our studies is specific for S2P$^{\Delta f}$-eDHFR antigen expression[22]. To underscore this point, no [^{18}F]FP-TMP signal was observed in mice vaccinated with eLNPs, which have been shown to be immunostimulatory, or in mice vaccinated with S2P alone[36–38].

Given the differences in metabolism, microbiota, and size between rodents and humans, measuring the biodistribution of S2P$^{\Delta f}$-eDHFR in a non-human primate is an important step in understanding the translational capacity of this PET reporter system. Whole body PET imaging was performed on the PennPET Explorer, an extended field-of-view PET scanner which permits high sensitivity dynamic imaging of the entire NHP[39]. High [^{18}F]FP-TMP signal was observed in the axillary LNs ipsilateral to vaccination on day 1. Interestingly, [^{18}F]FP-TMP signal was still present in the ipsilateral LNs on day 7 (NHP 1) and 8 (NHP 2), in contrast to the disappearance of LN signal by day 3 in mice. This data is consistent with a recent study which analyzed mRNA expression in the LNs of NHPs using IHC and found expression persisting to their terminal day 7 timepoint[33]. Importantly, the ipsilateral LN reached background levels by day 35 (NHP 1) and 99 (NHP 2). Given this data, we estimate that the vaccine is expressed for at least 8 days and less than 20 days with our formulation in translational models. While expression of S2P$^{\Delta f}$-eDHFR in the LNs remained consistent between NHPs, differences in muscle uptake and immune response were observed and may be a topic for further exploration in future studies. No [^{18}F]FP-TMP signal was observed in the LNs or the muscle of the control NHP vaccinated against *C. diff* (Data used in ref. 40), further validating the specificity of our system and its ability to detect precise trafficking and persistence of mRNA vaccine expression in vivo.

We also performed a series of immunogenicity tests that are important for this work, but also have implications for the use of eDHFR as a PET reporter gene in other systems (e.g., CAR T therapeutic systems)[28]. First, we quantified total IgG antibodies in mouse and NHP serum against spike and eDHFR following prime and boost vaccination. There were no antibodies detected against eDHFR, while a strong immune response was detected against spike. Next, we investigated antigen-specific T cells and their polyfunctionality with several

https://doi.org/10.1038/s41467-025-57446-w

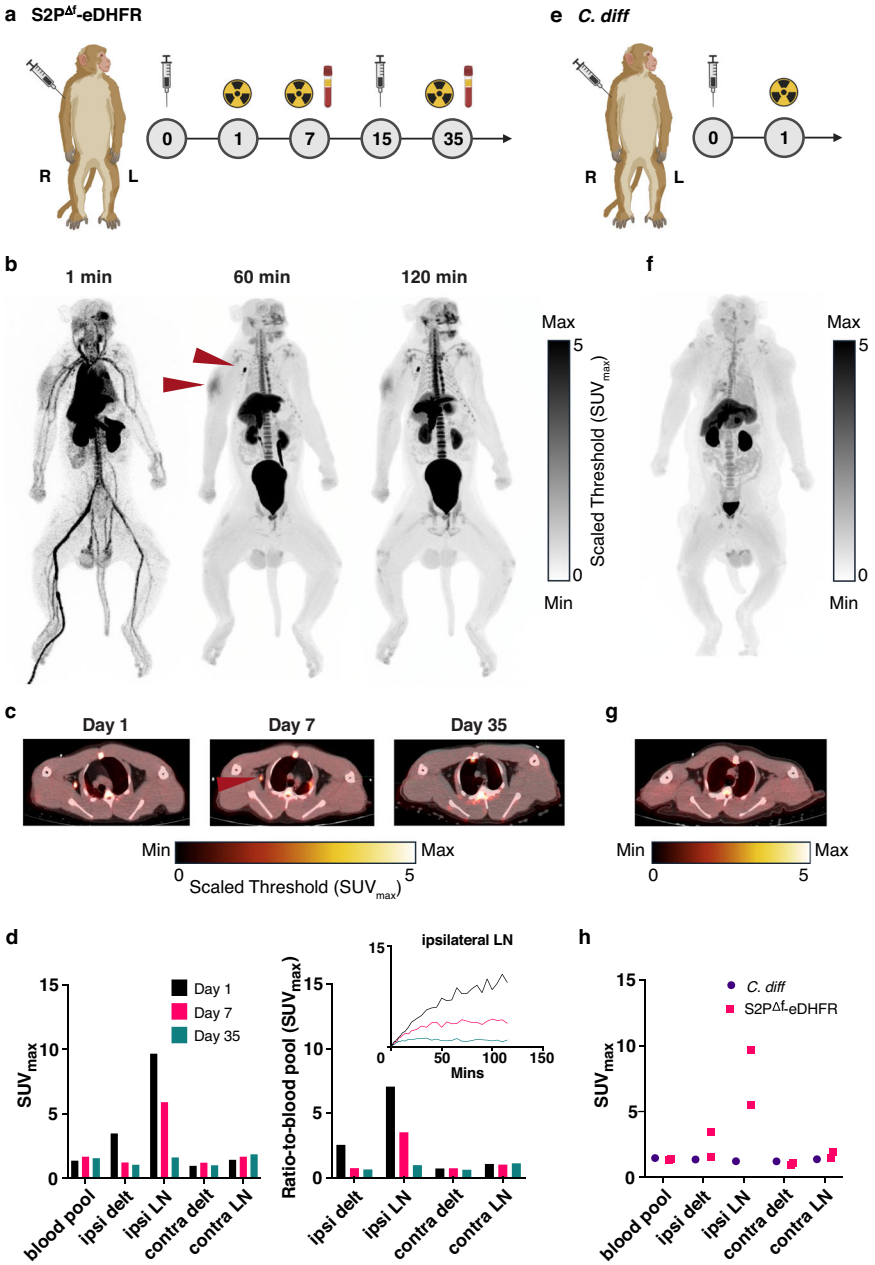

Fig. 6 | Dynamic whole body PET imaging in vaccinated NHPs. a Experimental timeline. NHP 1 was IM injected with S2P$^{\Delta f}$-eDHFR mRNA-LNPs in the right deltoid on day 0 and PET/CT imaged on day 1, 7, and 35. The NHP was boosted on day 15. Blood was collected on day 7 and 35 for analysis. **b** Dynamic PET/CT images of NHP 1 at 1, 60, and 120 min post [^{18}F]FP-TMP administration on day 1. Red arrows indicate [^{18}F]FP-TMP signal in the injected muscle and ipsilateral axillary LN. **c** Axial PET/CT slices through the axillary LNs at 60 min post [^{18}F]FP-TMP administration on day 1, 7, and 35. Red arrow indicates the ipsilateral axillary LN. **d** Quantification of [^{18}F]FP-TMP SUV$_{max}$ and SUV$_r$ in tissues of interest in NHP 1 at 60 min post [^{18}F]FP-TMP administration on day 1, 7, and 35. Inlet graph of the time activity curve of [^{18}F]FP-TMP SUV$_r$ in the ipsilateral axillary LN across timepoints. **e** Experimental timeline. An NHP was vaccinated with a *C. diff* mRNA-LNP vaccine in the right deltoid muscle on day 0 and PET/CT imaged on day 1. **f** Full body PET/CT image and **g** axial PET/CT slice through the axillary LNs at 60 min post [^{18}F]FP-TMP administration on day 1. **h** Quantification of [^{18}F]FP-TMP SUV$_{max}$ in tissues of interest in S2P$^{\Delta f}$-eDHFR vaccinated NHPs ($n = 2$) compared to the *C. diff* vaccinated NHP ($n = 1$) at 60 min post [^{18}F]FP-TMP administration on day 1. The ALC-0315 lipid was used in S2P$^{\Delta f}$-eDHFR NHP 1 and the ALC-307 lipid was used in NHP 2. **a**, **e** Created in BioRender. Sellmyer, M. (2025) https://BioRender.com/v54j936. Source data for panel (**d**, **h**) are provided as a Source Data file.

markers of immune response including IL-2, IFN-γ, and TNF-α. T cells stimulated with eDHFR peptides displayed little-to-no cross-reactivity while high levels of reactivity were seen against spike in both mice and NHPs. Finally, we evaluated cytotoxic T cell activity in vivo by assessing antigen-specific killing of eDHFR and spike peptide-loaded splenocytes. In mice vaccinated with S2P$^{\Delta f}$-eDHFR, cells loaded with eDHFR pooled-peptides were not killed, while robust killing was observed in the spike-loaded cells.

The finding that eDHFR is nonimmunogenic in mammalian systems is surprising given its bacterial origin and relatively low degree of homology (Supplementary Fig. 15). There are a couple of possible rationales for this. First, being C-terminal to the transmembrane protein S2P, eDHFR is expressed only intracellularly and may therefore evade immune recognition in the context of humoral antibody responses. However, GFP, which is a commonly used intracellular reporter protein, has been found to induce a cytotoxic T cell response

https://doi.org/10.1038/s41467-025-57446-w

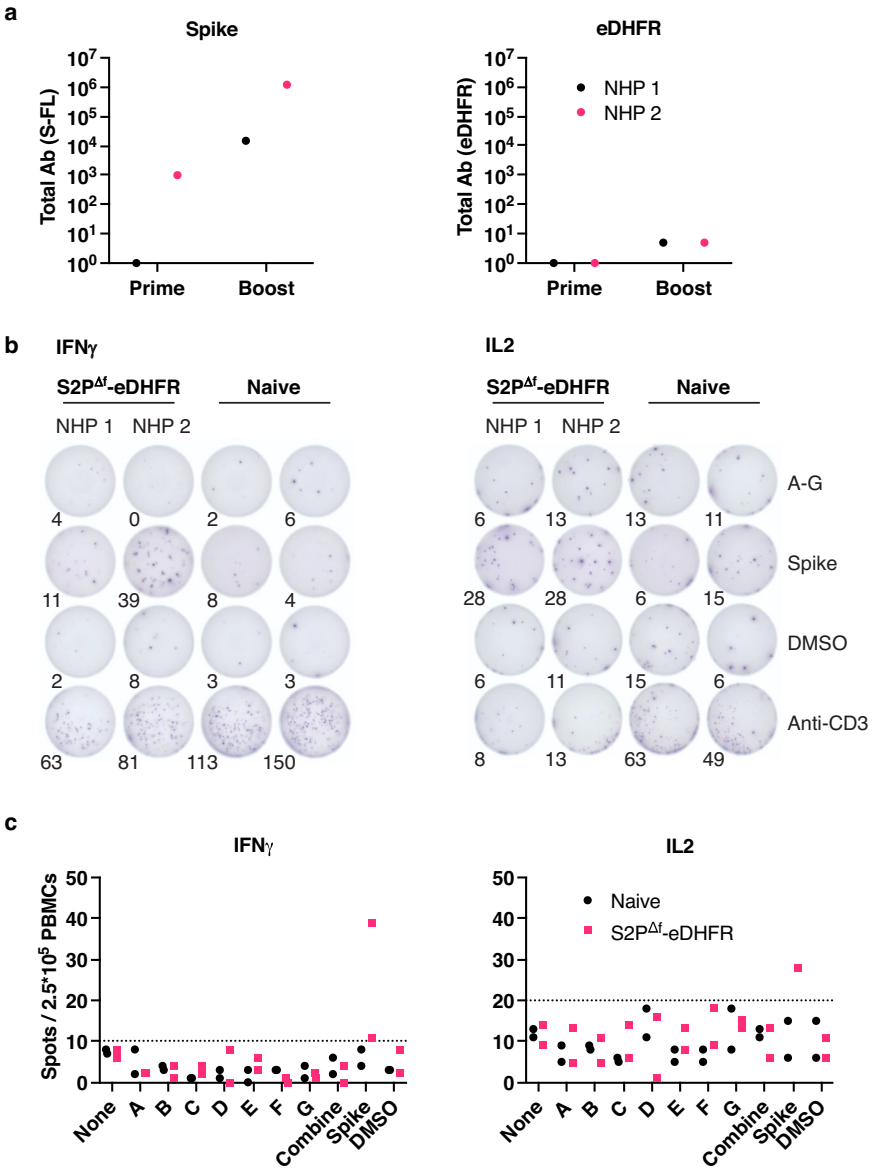

Fig. 7 | Quantification of humoral and cellular immune responses against spike and eDHFR in NHPs. a Total IgG antibodies against full length spike and eDHFR protein at prime and boost in NHP 1 and 2. $n = 2$ NHPs. **b** Representative plate wells with spot counts and **c** quantification from IFN-γ and IL-2 ELISPOT looking at cellular responses to eDHFR and spike peptides at boost. DMSO and Anti-CD3 were used as a negative and positive control, respectively. Dashed lines indicate maximum background levels for each cytokine. $n = 2$ NHPs per group. Source data are provided as a Source Data file.

in mice, suggesting other mechanisms may be conferring eDHFR immune evasion[41]. The observed lack of T cell reactivity towards eDHFR peptides is in alignment with previous work we have done where we tested the ability of a library of eDHFR peptides to elicit a memory immune response in primary human T cells. In this work, no response was detected against eDHFR, while a high response was detected against the FluM1 protein[28]. Because eDHFR and its homologs are widely expressed across bacterial species including those living in mammalian naso-oral epithelium and gut, there could be an acquired tolerance to commensal microorganism proteins such as eDHFR, while virulence factor proteins including FluM1 are much more immunogenic[42]. This data also suggests that the origin of peptide sequences and their degree of homology should not be a basis by which potential high value proteins are excluded from testing for animal and human use. More robust predictive models should be generated to test non-native sequences for their potential immunogenicity, especially as synthetic biology gains translational traction.

Some limitations to this technique exist, including its relative sensitivity. For example, low levels of SARS-CoV-2 spike protein have been detected in human LNs as long as 60 days after mRNA vaccination using IHC[43]. Given our NHP imaging data, it is unlikely that our PET reporter system has the sensitivity to detect these low levels of protein which potentially persist at late timepoints. Rather, we envision using this system as a tool to rapidly screen vaccine candidates for delivery to and expression in relevant tissue compartments, such as sites with a high concentration of APCs like the LNs[44]. Of note, eDHFR does not appear to express robustly as a standalone mRNA. When mice were vaccinated with eDHFR alone, uptake of [^{18}F]FP-TMP was not observed in any tissues of interest, suggesting the relatively lower expression of eDHFR compared with S2P$^{\Delta f}$-eDHFR may fall below the detection limits of our PET system (Supplementary Figs. 3-4). The poor expression of eDHFR may be due to factors affecting its mRNA stability including its length and non-optimized UTRs[45]. We have previously achieved suitable expression of eDHFR from lentiviral transduction where mRNA is constitutively

produced, in contrast to the transient nature of mRNA-LNPs[46]. Use of eDHFR as a standalone mRNA-encoded PET reporter will require further optimization. Another limitation includes the excretion pathways of [^{18}F] FP-TMP which may make it difficult to distinguish uptake in tissues in the abdominal region such as the inguinal LNs in mice. Fortunately, many other tissues of interest including heart, lung, brain, muscle, and other soft tissues have low background uptake in both mice and NHPs. Finally, while we report lower expression of S2P$^{\Delta f}$-eDHFR compared to S2P alone, the immune response against spike is indistinguishable between vaccination groups and consistent with previously reported IgG and T cell responses to the S2P vaccine in mice[47]. These results remain in S2P$^{\Delta f}$-eDHFR vaccinated NHPs, indicating that genetic fusion of eDHFR does not impact vaccine immunogenicity. Future studies which employ this imaging technique may require head-to-head comparison of the standalone and the eDHFR fusion antigen to assess any effect on overall expression or immunogenicity.

In future studies, we will use this strategy to evaluate therapeutic mRNA candidates. mRNA-delivered therapeutic proteins have different criteria for success and constraints including target engagement, expression longevity, and therapeutic threshold. Advances have already been made in this space in which targeting moieties to the LNP have been used to selectively deliver mRNA payloads to specific cell or tissue compartments[6,48]. Modifications to the mRNA transcript itself such as using optimized untranslated regions (UTRs) or circular and self-replicating RNAs are being actively explored to overcome the relatively short-lived expression kinetics and low levels of protein expression that are beneficial in vaccine settings but pose limitations in therapeutic applications[49–51].

Overall, this PET reporter approach is modular as eDHFR can be genetically fused to any protein of interest, encapsulated in any type of carrier system, and administered via any route to enable rapid head-to-head comparison of different coding transcripts, carriers, and formulations. Thus, both mRNA vaccines and therapeutics represent a rapidly expanding frontier which can be further accelerated through a robust noninvasive, nonimmunogenic, and modular mRNA-encoded PET reporter system.

Methods

mRNA synthesis and lipid nanoparticle encapsulation

The delta furin diproline modified SARS-CoV-2 spike glycoprotein (S2P$^{\Delta f}$) was genetically fused N-terminal to eDHFR and codon optimized. The full S2P$^{\Delta f}$-eDHFR sequence was then cloned into an in vitro transcription template plasmid containing a T7 promoter, 5′and 3′UTR regions, and a 100 nucleotide poly(A) tail. mRNA was synthesized and co-transcriptionally capped using the Megascript Transcription kit (Thermo Fisher, AMB 1334) and the CleanCap™ trinucleotide system (Trilink Biotechnologies), precipitated, and purified using a modified cellulose based chromatography method. Length and mRNA integrity were assessed using the Agilent Bioanalyzer 2100 system. Removal of double stranded RNA (dsRNA) contaminants was confirmed using dot blot and endotoxin levels were measured using the Genscript ToxiSensor chromogenic assay (<0.05 EU/mL). The S2P and S2P$^{\Delta f}$-eDHFR mRNA was stored frozen (1 mg/mL) at −20 °C in nuclease and pyrogen free water until use. mRNA was encapsulated into lipid nanoparticles as previously described[52]. A mixture of ionizable lipid (ALC-307, proprietary to Acuitas therapeutics, or ALC-0315), cholesterol, DSPC, and PEG-lipid was mixed in an ethanolic solution, and rapidly mixed with an aqueous phase containing the mRNA, dialyzed, and concentrated to 1 mg/mL, and stored at −80 °C until use. mRNA-LNPs were characterized for their hydrodynamic size, and polydispersity index (PDI), using dynamic light scattering (DLS), and the encapsulation efficiency and concentration measured using the RiboGreen RNA assay (Invitrogen, R11490). The hydrodynamic diameter of these mRNA-LNPs was approximately 71-78 nm with a PDI ranging from 0.05-0.13 and an encapsulation efficiency of ~97–98%.

Western blot

HEK293T cells (ATCC) were transfected with 25 μg of S2P or S2P$^{\Delta f}$-eDHFR mRNA using Lipofectamine MessengerMax (Invitrogen, LMRNA) according to manufacturer protocol. At 24 h, cells were harvested and solubilized in radioimmunoprecipitation assay (RIPA) lysis buffer (Cell Signaling Technology) with protease inhibitor (Roche Boehringer Mannheim) and incubated on ice for 30 min. Cell lysate was then centrifuged at 14,000 × *g* and the supernatant was stored at −80 °C until analysis. Total protein was quantified for each sample using a bicinchoninic acid (BCA) assay kit (Thermo Scientific). Samples were prepared at equal total protein concentration and loaded into a NuPage gel (Invitrogen, 4–12% Bis-tris) and run using NuPage MES Running Buffer (Invitrogen/Novex). Next, the SDS-page gel was transferred onto a polyvinylidene difluoride (PVDF) membrane (BioRad) activated by methanol and developed in NuPage transfer buffer (Invitrogen/Novex) with 20% methanol. The transfer was confirmed by Ponceau dye. Membranes were blocked in 5% Milk/TBS and washed with Tris-buffer saline (TBS) + 1% Tween (TBS-T). Next, the membrane was incubated with primary antibody (1:500, Sino Biological, 40590-MM05) in 5% Milk/TBS overnight. The membrane was washed and incubated with secondary antibody (1:1000, Cell Signaling Technology, 11967 s) in 5% Milk/TBS for 1 h. Recombinant SARS-CoV-2 spike S2 protein (Sino Biological, 40590-V08B) was used as a positive control. COX IV was blotted for as a loading control (1:2000, Cell Signaling Technologies, 11967 s). Following incubation, the membrane was washed and prepared for imaging using an enhanced chemiluminescence (ECL) kit (BioRad) and imaged on a ChemiDoc XRS+ system with Image Lab (BioRad).

Flow cytometry

HEK293T or DC2.4 cells (Sigma-Aldrich) were transfected with 25 μg of S2P or a molar ratio of S2P$^{\Delta f}$-eDHFR mRNA using Lipofectamine MessengerMax (Invitrogen, LMRNA). At 24 h, cells were lifted with versene solution (EDTA), resuspended in FACS buffer (5% FBS in PBS), and incubated with an Alexa Fluor 647 conjugated (Invitrogen, A20186) SARS-CoV-2 spike S2 mouse monoclonal antibody (Sino Biological, 40590-MM05) for 1 h at 4 °C. Stained cells were analyzed on a BD LSR II flow cytometer for surface expression of S2P until 10,000 events were recorded. All flow data were analyzed using FlowJo.

[^{18}F]FP-TMP cell uptake study

HEK293T cells were transfected with 25 μg of S2P or S2P$^{\Delta f}$-eDHFR mRNA using Lipofectamine MessengerMax and resuspended using versene solution (EDTA). Following overnight transfection, cells were incubated with 2×10^6 counts per minute (CPM) of [^{18}F]FP-TMP per 1×10^6 cells in the presence or absence of 10 μM TMP in complete media. Following 1 h incubation, cells were pelleted and washed 3 times with 1% DMSO in cold PBS. Finally, cells were resuspended in cold PBS and split into 3 technical replicates. [^{18}F]FP-TMP uptake was quantified on a gamma counter (Perkin Elmer) and analyzed by dividing the [^{18}F] counts in each experimental condition by the [^{18}F] counts of the total incubated dose (%ID/10^6 cells). [^{18}F]FP-TMP was synthesized as we have performed previously[22]. The specific activity is 19442 ± 12277 Ci/mmol or 719354 ± 454249 GBq/mmol.

Mice

Female Balb/c mice (*Mus musculus*) between 8 and 12 weeks of age were purchased from Charles River for experiments. Mice were housed according to University of Pennsylvania's University Laboratory Animal Resources (ULAR) and Institutional Animal Care and Use Committee (IACUC) protocol. Temperature was maintained at 20–24 °C and relative humidity was between 30 and 70% on a standard 12 h light/dark cycle, 7 days a week. All mouse imaging and immunogenicity studies were performed in accordance with University of Pennsylvania's ULAR and IACUC guidelines (IACUC 805477 and 803941, respectively).

Small animal PET/CT imaging

Adult female Balb/c mice were vaccinated IM in the right hindlimb with 10 μg of mRNA-LNPs. On imaging days, mice were injected intravenously (IV) with 200 μCi (7.4 MBq) of [^{18}F]FP-TMP. Following a 2 h uptake, mice were anesthetized under 2% isoflurane in pure O_2 for PET/CT imaging on a small animal PET scanner (Molecubes). Quantitative analysis was performed using MIM (MIM Software). A 3D ROI was drawn around tissues of interest on the CT image and the maximum SUV (SUV_{max}) was quantified.

ELISA

96-well High Bind Stripwell™ Corning 96 Well Clear Polystyrene Microplates plates were coated overnight with 1 μg/mL of purified spike full length (SinoBiological, 40589-V08H8) and recombinant eDHFR (Gift from Ronen Marmorstein Laboratory, University of Pennsylvania, Philadelphia, PA). Plates were washed three times with wash buffer (0.5% Tween-20 in PBS) and blocked with a solution of heat inactivated, IgG depleted, protease free bovine serum albumin (2% w/v BSA in PBS) for 2 h at room temperature. After blocking, plates were washed three times, and mouse or NHP serum was serially diluted 1:3 in the blocking solution and incubated for two hours at room temperature. Plates were washed three times before the addition of horseradish peroxidase-conjugated anti-mouse (1:10,000, Abcam, AB98717) or goat anti-rhesus IgG (1:20,000, SouthernBiotech, 13605) secondary antibody against total IgG in blocking buffer. Plates were incubated for 1.5 h at room temperature and washed three times before the addition of tetramethylbenzidine (TMB, Seracare, 5120-0049 and 5120-0038) substrate solution for 10 min. The reaction was stopped by adding 2 N sulfuric acid, and the absorbance was measured at 450 nm using a SpectraMax™ 190 microplate reader immediately. Antigen-specific antibody end-point dilution titer was defined as the highest dilution of serum with an OD greater than the cut-off OD value determined using the Frey Method[53].

T cell polyfunctionality

To isolate T cells, spleens were collected and processed as single cells. Cells were filtered using a 70 μm cell strainer in complete RPMI 1640, centrifuged, and red blood cells were lysed in ACK lysis buffer to obtain a clear single cell suspension. To measure antigen-specific T cells, 2 million splenocytes were stimulated with spike or eDHFR peptide pools in a FACS tube with 2 mg/mL anti-CD28 providing co-stimulation for 6 h at 37 °C and 5% CO_2. For comparison between S2P$^{\Delta f}$-eDHFR and eLNP, splenocytes were exposed to a combined pool of spike peptides or individual eDHFR peptides (A-G) which covered the entire length of the protein (15mers, 4 amino acid gap, 11 amino acid overlap, >90% purity by LC/MS). For comparison between eDHFR, S2P$^{\Delta f}$-eDHFR and S2P, splenocytes were exposed to combined pools of spike or eDHFR peptides. All peptides regardless of pooled or individual were at a concentration of 2.5 μg/mL. Stimulations proceeded for 1 h before addition of 5 mg/mL brefeldin A, 2 mM monensin, and 5 mg/mL anti-CD107α Alexa Fluor 647 for 5 h. DMSO served as a negative control and the combination of 50 mg/mL phorbol 12-myristate 13-acetate and 1 mg/mL ionomycin served as a positive control as needed. After a total of 6 h, samples were washed with PBS, stained with Live/Dead Aqua for 10 min at room temperature, blocked using anti-mouse CD16/32 antibody for 20 min at 4 °C, and stained extracellularly for 30 min using antibodies at 4 °C in the dark. Cells were washed in FACS buffer (2% FBS in PBS), fixed and permeabilized using the Cytofix/Cytoperm kit, and stained intracellularly using antibodies for 30 min at 4 °C in the dark. Following intracellular staining, cells were washed twice, fixed with 250 μL of 1% paraformaldehyde (in FACS buffer) and samples were acquired on a BD LSR II equipped with 4 laser lines and 18 PMTs. Flow data were analyzed using FlowJo. The gating strategy, antibody list, and catalog numbers, are provided (Supplementary Fig. 7; Supplementary Table 3).

In vivo cytotoxicity assay

CFSE (Cell trace CFSE, Invitrogen, C34554) was resuspended in DMSO and diluted in PBS to prepare 7 μM and 0.7 μM solutions. To prepare CFSE pulsed cells, naïve mice ($n = 5$) were sacrificed and spleens were harvested to prepare splenocyte single cell suspension as described before. Cells were counted, pelleted, and resuspended in 7 μM CFSE solution at 5×10^7 cells/mL of CFSE solution to prepare CFSE^{hi} (high pulse) cells. Similarly, CFSE^{lo} (low pulse) cells were prepared with 0.7 μM CFSE solution. Both cell suspensions were incubated at 37 °C in the dark for 15 min, centrifuged and washed with RPMI 1640 media. Both cell suspensions were resuspended at 2.5×10^7 cells/mL in media and CFSE^{lo} cells were kept on ice until later.

CFSE^{hi} cells were split into 2 groups for stimulation with spike or eDHFR peptide pools (combined, 2.5 μg/mL each peptide) and incubated at 37 °C for 90 min in the dark to obtain CFSE$^{hi\text{-}spike}$ and CFSE$^{hi\text{-}eDHFR}$, respectively. CFSE^{lo} and both CFSE^{hi} cells were washed with RPMI 1640 media, resuspended in complete media at 5×10^7 cells/mL and counted. Two different cell suspensions were prepared by mixing (1) CFSE^{lo} and CFSE$^{hi\text{-}spike}$ cells and, (2) CFSE^{lo} and CFSE$^{hi\text{-}eDHFR}$ cells in a 1:1 ratio. Both cell suspensions were pelleted and resuspended in PBS (100 μL/mouse) and 4×10^6 total cells/mouse (2×10^6 CFSE^{lo} and 2×10^6 CFSE^{hi}) were injected IV into mice 12 days after second vaccination.

Mice were sacrificed 24 h after the CFSE labeled cells were injected; spleens were collected and splenocyte single cell suspensions were prepared. Cells were fixed in 1% paraformaldehyde (in FACS buffer) and acquired on LSR II at 515 nm until 25,000 CFSE positive events were recorded. The ratio of CFSE^{hi}:CFSE^{lo} was used to determine the cytotoxic T cell activity where peptide-loaded CFSE^{hi} cells are killed by the antigen-specific T cells while the unstimulated CFSE^{lo} cells were not killed. A CFSE^{lo}:CFSE^{hi} ratio of 1:1 indicates no killing while a reducing proportion of CFSE^{hi} cells is an indicator of T cell killing.

NHP PET/CT imaging

Two rhesus monkeys (*Macaca mulatta*) were vaccinated IM in the right deltoid with 200 μg of S2P$^{\Delta f}$-eDHFR mRNA-LNPs on day 0 and boosted on day 15. A single rhesus monkey was vaccinated with 200 μg of a *Clostridium difficile* (*C. diff*) tetravalent mRNA-LNP vaccine[40]. PET/CT imaging was performed on a clinical grade PET scanner (PennPET Explorer). Prior to imaging, monkeys were fasted overnight and anesthetized with ketamine (4 mg/kg) and dexmedetomidine (0.05 mg/kg) for transport to the scanner facility. During imaging, monkeys were maintained on 1–2% isoflurane in pure O_2 via intubation, vital signs were monitored, and body temperature was sustained using a circulating water heating pad and blankets. Monkeys were injected with 3–3.5 mCi (111-129.5 MBq) of [^{18}F]FP-TMP radiotracer at time 0 and a series of dynamic images were acquired over 120 min with the following bins: 12×10, 2×30, 4×60, 2×120, 3×180, and 20×300 (images x seconds). For image analysis, images were reconstructed with 2 mm voxels and [^{18}F]FP-TMP uptake was normalized to the height and weight of the monkey. A 3D ROI was drawn on the CT images over tissues of interest to determine the SUV_{max}. At the time of experimentation, the NHP ages were as follows: S2P$^{\Delta f}$-eDHFR NHP 1, 9 years; NHP 2, 17 years; *C. diff*, 20 years. All NHP studies were performed in accordance with University of Pennsylvania's ULAR and IACUC guidelines (IACUC 805073).

ELISPOT

Rhesus peripheral mononuclear cells (PBMCs) were isolated from blood samples through density gradient centrifugation. In brief, 20–30 mL of peripheral blood was centrifuged at $1600 \times g$ for 30 min

to collect the plasma. The rest of the sample was diluted with PBS in 1:1 ratio. Diluted peripheral blood samples were loaded on the Ficoll-Paque in a 2:1 ratio and centrifuged at 385 × *g* for 40 min with the acceleration and brake off. PBMC-enriched buffy coat was harvested and washed twice with PBS. PBMCs were cryopreserved with 10% DMSO in FBS for future analysis.

ELISPOT assays were performed using the Monkey IFN-γ ELISpot PLUS kit (Mabtech, 3421M-4APW) or IL-2 ELISpot PLUS kit (Mabtech, 3445M-4APW) according to manufacturer protocol. In brief, cryopreserved rhesus macaque PBMCs were thawed out and rested in complete culture medium (10% FBS, 12.5 mM HEPES, 1X non-essential amino acid, 1X sodium pyruvate and 55 μM 2-mercaptoethanol in RPMI 1640) at 37 °C for 16 h. Next, 2.5×10^5 rested PBMCs were stimulated with various peptide pools (2.5 μg/mL) for 24 (IL-2) or 48 h (IFN-γ). For the anti-CD3 treatment, 2.5×10^4 cells were stimulated with 1:100 diluted antibodies provided by the kit. Cells were removed after stimulation through washing with PBS and plates were incubated with biotin-conjugated detection antibody for 2 h. Plates were washed with PBS and incubated with streptavidin-conjugated alkaline phosphatase (ALP) for 1 h. After incubation, plates were washed and developed with filtered BCIP/NBT substrate solution. The reaction was stopped by washing extensively with water. Plates were dried at room temperature for 16 h and measured by ELISPOT reader using S6 Universal M2 (ImmunoSpot, CTL).

Statistical analysis

Statistical parameters are stated in the figure legends. All statistical analyses were performed in Prism 10 (GraphPad). A p-value of <0.05 was considered to be statistically significant. Blinding and randomization were not used. An ordinary one-way ANOVA with Tukey's multiple comparisons test was performed to evaluate differences among groups. For comparisons involving two independent variables, a two-way ANOVA with either Tukey's or Sidak's multiple comparisons test was used. An unpaired, two-tailed *t* test was applied for comparisons between two treatment groups.

Reporting summary

Further information on research design is available in the Nature Portfolio Reporting Summary linked to this article.

Data availability

The data generated in this study are provided in the Supplementary Information/Source Data file. Source data are provided with this paper.

References

1. Pardi, N., Hogan, M. J., Porter, F. W. & Weissman, D. mRNA vaccines - a new era in vaccinology. *Nat. Rev. Drug. Discov.* **17**, 261–279 (2018).
2. Sahin, U., Karikó, K. & Türeci, Ö. mRNA-based therapeutics-developing a new class of drugs. *Nat. Rev. Drug. Discov.* **13**, 759–780 (2014).
3. Semple, S. C. et al. Rational design of cationic lipids for siRNA delivery. *Nat. Biotechnol.* **28**, 172–176 (2010).
4. Karikó, K., Buckstein, M., Ni, H. & Weissman, D. Suppression of RNA recognition by Toll-like receptors: The impact of nucleoside modification and the evolutionary origin of RNA. *Immunity* **23**, 165–175 (2005).
5. Cheng, Q. et al. Selective organ targeting (SORT) nanoparticles for tissue-specific mRNA delivery and CRISPR–Cas gene editing. *Nat. Nanotechnol.* **15**, 313–320 (2020).
6. Rurik, J. G. et al. CAR T cells produced in vivo to treat cardiac injury. *Science* **375**, 91–96 (2022).
7. Ols, S. et al. Route of vaccine administration alters antigen trafficking but not innate or adaptive immunity. *Cell. Rep.* **30**, 3964–3971.e7 (2020).
8. Gambhir, S. S. et al. Imaging adenoviral-directed reporter gene expression in living animals with positron emission tomography. *Proc. Natl. Acad. Sci. USA* **96**, 2333–2338 (1999).
9. Serganova, I. & Blasberg, R. G. Molecular imaging with reporter genes: Has its promise been delivered? *J. Nucl. Med.* **60**, 1665–1681 (2019).
10. Pardi, N. et al. Expression kinetics of nucleoside-modified mRNA delivered in lipid nanoparticles to mice by various routes. *J. Control. Release* **217**, 345–351 (2015).
11. Kauffman, K. J. et al. Rapid, single-cell analysis and discovery of vectored mRNA transfection in vivo with a loxP-Flanked tdTomato reporter mouse. *Mol. Ther. Nucleic Acids* **10**, 55–63 (2018).
12. Concilio, S. C., Russell, S. J. & Peng, K. W. A brief review of reporter gene imaging in oncolytic virotherapy and gene therapy. *Mol. Ther. Oncolytics* **21**, 98–109 (2021).
13. Keu, K. V. et al. Reporter gene imaging of targeted T cell immunotherapy in recurrent glioma. *Sci. Transl. Med.* **9**, 2196 (2017).
14. Skourti, E. et al. Spatiotemporal quantitative microRNA-155 imaging reports immune-mediated changes in a triple-negative breast cancer model. *Front. Immunol.* **14**, 1180233 (2023).
15. Gurung, S. et al. mRNA therapy corrects defective glutathione metabolism and restores ureagenesis in preclinical arginino-succinic aciduria. *Sci. Transl. Med.* **16**, 1334 (2024).
16. Wong, P. et al. PET imaging of 64Cu-DOTA-scFv-anti-PSMA lipid nanoparticles (LNPs): Enhanced tumor targeting over anti-PSMA scFv or untargeted LNPs. *Nucl. Med. Biol.* **47**, 62–68 (2017).
17. Lindsay, K. E. et al. Visualization of early events in mRNA vaccine delivery in non-human primates via PET–CT and near-infrared imaging. *Nat. Biomed. Eng.* **3**, 371–380 (2019).
18. Sellmyer, M. A. et al. Imaging CAR T cell trafficking with eDFHR as a PET reporter gene. *Mol. Ther.* **28**, 42–51 (2019).
19. Lee, I. K. et al. Imaging sensitive and drug-resistant bacterial infection with [11C]-trimethoprim. *J. Clin. Invest.* **132**, 1–12 (2022).
20. Chen, Z., Jing, C., Gallagher, S. S., Sheetz, M. P. & Cornish, V. W. Second-generation covalent TMP-tag for live cell imaging. *J. Am. Chem. Soc.* **134**, 13692–13699 (2012).
21. Jacome, D. A. et al. A chemical approach for programmable protein outputs based on engineered cell interactions. *ACS Chem. Biol.* **16**, 52–57 (2021).
22. Sellmyer, M. A. et al. Bacterial infection imaging with [18F]fluoropropyl-trimethoprim. *Proc. Natl. Acad. Sci. USA* **114**, 8372–8377 (2017).
23. Rybakova, Y. et al. mRNA delivery for therapeutic anti-HER2 antibody expression in vivo. *Mol. Ther.* **27**, 1415–1423 (2019).
24. Collén, A. et al. VEGFA mRNA for regenerative treatment of heart failure. *Nat. Rev. Drug Discov.* **21**, 79–80 (2022).
25. Aliprantis, A. O. et al. A phase 1, randomized, placebo-controlled study to evaluate the safety and immunogenicity of an mRNA-based RSV prefusion F protein vaccine in healthy younger and older adults. *Hum. Vaccin. Immunother.* **17**, 1248–1261 (2021).
26. Lokugamage, M. P. et al. Optimization of lipid nanoparticles for the delivery of nebulized therapeutic mRNA to the lungs. *Nat. Biomed. Eng.* **5**, 1059–1068 (2021).
27. O'Doherty, J. et al. 18F-tetrafluoroborate, a PET probe for imaging sodium/iodide symporter expression: Whole-body biodistribution, safety, and radiation dosimetry in thyroid cancer patients. *J. Nucl. Med.* **58**, 1666–1671 (2017).
28. Lee, I. K. et al. A genetically encoded protein tag for control and quantitative imaging of CAR T cell therapy. *Mol. Ther.* **31**, 3564–3578 (2023).
29. Nerella, S. G. et al. PET reporter systems for the brain. *Trends Neurosci.* **46**, 941–952 (2023).

30. Polack, F. P. et al. Safety and efficacy of the BNT162b2 mRNA Covid-19 vaccine. *N. Engl. J. Med.* **383**, 2603–2615 (2020).
31. Huang, Y., Yang, C., Xu, X. F., Xu, W. & Liu, S. W. Structural and functional properties of SARS-CoV-2 spike protein: potential antivirus drug development for COVID-19. *Acta Pharmacol. Sin.* **41**, 1141–1149 (2020).
32. Lemdani, K. et al. Distinct dynamics of mRNA LNPs in mice and nonhuman primates revealed by in vivo imaging. *npj Vaccines* **9**, 113 (2024).
33. Hassett, K. J. et al. mRNA vaccine trafficking and resulting protein expression after intramuscular administration. *Mol. Ther. Nucleic Acids* **35**, 102083 (2024).
34. Rahman, W. T. et al. The impact of infection and inflammation in oncologic 18F-FDG PET/CT imaging. *Biomed. Pharmacother.* **117**, 109168 (2019).
35. Bernstine, H. et al. Axillary lymph nodes hypermetabolism after BNT162b2 mRNA COVID-19 vaccination in cancer patients undergoing 18F-FDG PET/CT: A cohort study. *Clin. Nucl. Med.* **46**, 396–401 (2021).
36. Lee, Y., Jeong, M., Park, J., Jung, H. & Lee, H. Immunogenicity of lipid nanoparticles and its impact on the efficacy of mRNA vaccines and therapeutics. *Exp. Mol. Med.* **55**, 2085–2096 (2023).
37. Karikó, K. et al. Incorporation of pseudouridine into mRNA yields superior nonimmunogenic vector with increased translational capacity and biological stability. *Mol. Ther.* **16**, 1833–1840 (2008).
38. Ndeupen, S. et al. The mRNA-LNP platform's lipid nanoparticle component used in preclinical vaccine studies is highly inflammatory. *iScience* **24**, 103479 (2021).
39. Pantel, A. R. et al. PennPET explorer: Human imaging on a whole-body imager. *J. Nucl. Med.* **61**, 144–151 (2020).
40. Alameh, M.-G. et al. A multivalent MRNA-LNP vaccine protects against clostridioides difficile infection. *Science* **386**, 69–75 (2024).
41. Ansari, A. M. et al. Cellular GFP toxicity and immunogenicity: Potential confounders in in vivo cell tracking experiments. *Stem Cell Rev. Rep.* **12**, 553–559 (2016).
42. Zheng, D., Liwinski, T. & Elinav, E. Interaction between microbiota and immunity in health and disease. *Cell Res.* **30**, 492–506 (2020).
43. Röltgen, K. et al. Immune imprinting, breadth of variant recognition and germinal center response in human SARS-CoV-2 infection and vaccination. *Cell* **185**, 1–16 (2022).
44. Liang, F. et al. Efficient targeting and activation of antigen-presenting cells in vivo after modified mRNA vaccine administration in rhesus macaques. *Mol. Ther.* **25**, 2635–2647 (2017).
45. Leppek, K. et al. Combinatorial optimization of mRNA structure, stability, and translation for RNA-based therapeutics. *Nat. Commun.* **13**, 1536 (2022).
46. Etersque, J. M. et al. Regulation of eDHFR-tagged proteins with trimethoprim PROTACs. *Nat. Commun.* **14**, 7071 (2023).
47. Prompetchara, E. et al. Immunogenicity and protective efficacy of SARS-CoV-2 mRNA vaccine encoding secreted non-stabilized spike in female mice. *Nat. Commun.* **14**, 2309 (2023).
48. Breda, L. et al. In vivo hematopoietic stem cell modification by mRNA delivery. *Science* **381**, 436–443 (2023).
49. Yang, J. et al. Intratumoral delivered novel circular mRNA encoding cytokines for immune modulation and cancer therapy. *Mol. Ther. Nucleic Acids* **30**, 184–197 (2022).
50. Vogel, A. B. et al. Self-amplifying RNA vaccines give equivalent protection against influenza to mRNA vaccines but at much lower doses. *Mol. Ther.* **26**, 446–455 (2018).
51. Asrani, K. H. et al. Optimization of mRNA untranslated regions for improved expression of therapeutic mRNA. *RNA Biol.* **15**, 756–762 (2018).
52. Maier, M. A. et al. Biodegradable lipids enabling rapidly eliminated lipid nanoparticles for systemic delivery of RNAi therapeutics. *Mol. Ther.* **21**, 1570–1578 (2013).
53. Frey, A., Di Canzio, J. & Zurakowski, D. A statistically defined endpoint titer determination method for immunoassays. *J. Immunol. Methods* **221**, 35–41 (1998).

Acknowledgements

We thank the members of the Small Animal Imaging Facility (Eric Blankenmeyer) and the Cyclotron (Hsiaoju Lee, Shihong Li, Alexander Schmidt); Kimberly Edwards and Kexiang Xu for help with the animal injections; and Jonathan Pham for helpful discussions and comments. M.A.S is supported by the National Institute of Health Office of the Director Early Independence Award (DP5-OD26386), NIGMS (R01GM150804), Burroughs Wellcome Fund Career Award for Medical Scientists (CAMS), and CRI Lloyd J. Old STAR (CRI5589). G.S.B. is supported by the J. Crayton Pruitt Foundation.

Author contributions

M.A.S., G.S.B., and M.G.A. conceptualized the project. M.A.S., G.S.B., M.G.A., G.D., and Y.P. contributed to the experimental design. G.S.B., G.D., M.G.A., Y.P., C.H., J.M.E., A.C., H.N., and B.D. performed experiments, analyzed data, and interpreted results. H.S., M.G.A, D.W., and Y.T. provided material. Q.C. provided statistical analysis oversight. D.W., M.L., M.G.A., and R.H.M. provided external oversight and resources. M.G.A. and M.A.S. managed the project. G.S.B. visualized the data and wrote the manuscript. All authors contributed to the final manuscript.

Competing interests

M.A.S. and R.H.M. are cofounders of Vellum Biosciences and inventors on intellectual property (IP) related to the PET imaging of genetic therapies. A provisional patent related to this work has been filed with the USPTO (63/637301) on which M.A.S., G.B., M.G.A., G.D., R.H.M., and D.W. are inventors. Y.T. is an employee of Acuitas, holds equity at Acuitas, and is cited on multiple patents for the use of lipid nanoparticles in vaccines and therapeutics. M.G.A. and D.W. are cited on multiple patents for the use of lipid nanoparticles, vaccines and therapeutics. M.G.A. serves as a scientific adviser for AfriGen Biologics, and also has an ownership stake in RNA Technologies. D.W. serves as a scientific advisor for Arcturus Therapeutics, Cabaletta Bio, and Versatope Therapeutics, and also has ownership stakes in Capstan Therapeutics, Orbital Therapeutics, Zipcode Bio, and RNA Technologies. D.W. receives royalties from CellScript and Capstan Therapeutics. All senior authors declare no conflicts of interest. In accordance with the University of Pennsylvania and Children's Hospital of Philadelphia policies and procedures and our ethical obligations as researchers, we have disclosed those interests fully to the University of Pennsylvania and the Children Hospital of Philadelphia and have in place an approved plan for managing any potential conflicts arising from licensing of the patents.

Additional information

Supplementary information The online version contains supplementary material available at https://doi.org/10.1038/s41467-025-57446-w.

Correspondence and requests for materials should be addressed to Mohamad-Gabriel Alameh or Mark A. Sellmyer.

Peer review information *Nature Communications* thanks the anonymous reviewers for their contribution to the peer review of this work. A peer review file is available.